CORE FORMATION: A NEW MODELLING APPROACH

Ruth Ziethe[1], T. Spohn[1], and S. Turek[2]

[1]Institut für Planetologie, University of Münster, 48149 Münster, Germany
[2]Institute of Applied Mathematics, University of Dortmund, 44227 Dortmund, Germany

ABSTRACT

Core formation in terrestrial planets is still not well understood although this process is of importance for our understanding of the thermal evolution of a planet and the history of its magnetic field. Because core formation is among the earliest processes in planet formation and evolution, the initial conditions for thermal evolution models are, to a significant extent, determined by this process. The initial temperature of the core and its state are determined by the amount of energy dissipated during core formation. One possible scenario for the formation of a planetary core is the settling of liquid iron from a solid matrix (Stevenson, 1990). Assuming that a planet in the late state of accretion has a magma ocean, there soon will form a layer of molten iron at the bottom of the magma ocean. Since the iron has a higher density than the underlying planetary mantle, it will probably sink due to Rayleigh–Taylor instability. According to Woidt (1978) the sinking iron will attain the shape of spheres because the viscosity of the liquid iron should be much smaller than that of silicates. We model the Stokes falling of an iron sphere through a silicate mantle with temperature dependent viscosity of the mantle material by using a finite element code (FEATFLOW) written by Turek (1998). We solve the incompressible Navier–Stokes equation coupled with the energy and mass equation. With these models the effect of the temperature dependence of the silicate rock viscosity on the differentiation rate and the temperature of the core after core formation can be estimated.

Key words: Core formation, planetary interiors, Computational Fluid Dynamics.

1. INTRODUCTION

Core formation is an important albeit still little understood process of differentiation for terrestrial planets and satellites. While it is still not entirely clear whether or not the Moon has a small iron core of perhaps 400 km radius (Konopliv *et al.*, 1998) it is widely held that the terrestrial planets all have iron rich cores. For Mars this is implied by the moment of inertia factor of 0.365 that requires a core (Sohl & Spohn, 1997; Spohn *et al.*, 1998). For Mercury, a core is necessary to explain the high density of the planet of $5340\,\mathrm{kg\,m^3}$ (Vila *et al.*, 1988). While the Earth's core is well established, there is no direct evidence for a core in Venus. But it is commonly assumed that Venus has a core in analogy to its sister planet Earth. Even the inner three of the Galilean satellites of Jupiter Io, Europa, and Ganymede are likely to have cores as the recent gravity data from the Galileo mission suggest (see for a recent review Sohl *et al.*, 2002).

It is commonly assumed that core formation is among the earliest processes in the interior of a planet. W-Hf isotope studies show that for Mars and Earth core formation occurred soon after accretion and took only a few tens of million years to complete (Lee & Halliday, 1997; Halliday & Lee, 1999). However, there is some indirect evidence that core formation in the Galilean satellites may have taken much longer, perhaps gigayears (Spohn & Breuer, 1998).

Core formation may have been strongly affected or have even been triggered by collisions not only between planets and small bodies like asteroids or comets but also between planet sized objects. Giant collisions may have melted large parts of a planet or may have even removed its outer shell by vaporization, a possibility cited for the early Earth and Mercury. For Earth, the vaporized material may have helped to form the Moon (Cameron, 1997) and for Mercury vaporization of part of its early outer silicate shell may explain its unusually high density (Cameron *et al.*, 1988). Large amounts of energy were probably dissipated as heat in the very first part of planetary evolution in its outer layers which helped not only to melt the iron but also may have facilitated its path to the deep interior by weakening the solid material of the protoplanet.

1.1. Scenarios for core formation

It is, of course, possible that the core forms during heterogeneous accretion in which case a particular

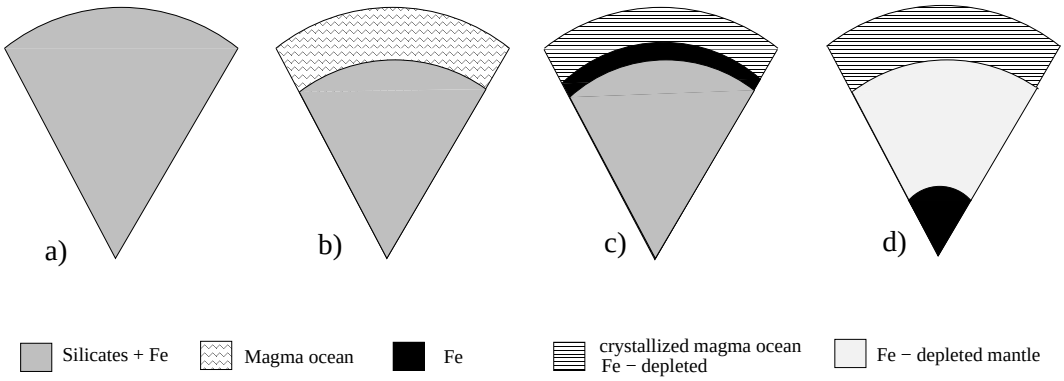

Figure 1. Simple core formation sketch. a) homogeneously accreted protoplanet, b) during heavy bombardement, the outer shell melts because of the conversion from kinetic energy of impactors to heat and a magma ocean is formed, c) light and heavy (mainly iron) components separate in the magma ocean, the magma ocean freezes and is layered afterwards, d) because of the unstable state of a heavier medium overlying a lighter one, the iron sinks to the planet's centre in a Rayleigh–Taylor instability. On the way to the centre of the planet the migrating iron collects iron from the deeper mantle (possibly migrated through pores)

core-formation-model is not required. Although heterogeneous planet formation cannot be disproved by pure observation it is nevertheless improbable due to many reasons as discussed in Boss *et al.* (1989), Wasson (1988), Ringwood (1979, 1984), Jacobs (1987). Therefore, we assume in this paper that the planet formed homogeneously and that the core formed later through planet-wide differentiation. According to Stevenson (1990) the following scenarios for the separation of iron from silicate material are conceivable:

Percolative core formation. The planetary mantle is assumed to be a porous medium – porous on the scale of crystal size – containing finely distributed liquid iron. For a sufficiently large permeability the iron melt is able to migrate through the silicate matrix to form larger melt bodies. The permeability depends on a variety of parameters such as the surface energy between the melt and the solid phases and on the degree of melting or melt concentration. The difference in surface energy between the phases largely determines the dihedral angle of the melt pocket. Only for dihedral angles smaller than 60 degree can an interconnected melt film between the solid grains form and allow an effective transport of the melt by percolation. For larger angles the droplets will stay isolated and will be trapped by the solid. Unfortunately, the dihedral angle between iron melt and low pressure silicate phases ($< \approx 3\,\mathrm{GPa}$) of is commonly larger than 60 degrees (van Bargen & Waff, 1986) and a continous melt film is not likely to be possible. For perovskite, the dihedral angle seems to be smaller than 60 degrees (van Bargen & Waff, 1988), meaning that as argued by Stevenson (1990) the existence of a perovskite layer is a condition for core formation with the percolation model. However, if perovskite is necessary, then this model of core formation can only work for the big terrestrial planets Earth and Venus in which the pressure increases rapidly enough for a thick lower perovskite protocore to form. In Mars, the depth to the perovskite protocore will only be approximately equal to the depth of the present core-mantle boundary (Sohl & Spohn, 1997). In any case, the percolation model allows for a hot initial core (after core formation) because the surface to volume ratio for the melt is large and effective heating due to viscous dissipation is possible.

Core formation by rainfall. This model assumes that the planet is completely or almost completely molten after accretion . The iron can easily form drops, which will sink and form a core in the centre of the planet. Although this core formation mechanism is easily understood, it is perhaps rarely applicable since it is difficult to see how terrestrial planets and smaller satellites could ever have been completely molten. An exception is the Moon for which isotope data suggest that at least half the volume was molten (Zitat, Palme?) probably as a consequence of its formation from a hot vapour cloud.

Core formation by diapirism. In this model kilometer sized iron melt blobs sink through the solid silicate mantle due to their higher density. The sinking is possible because the solid mantle on long enough time scales (millions of years) undergoes solid state creep and behaves like a very viscous fluid. The sinking starts through a Rayleigh–Taylor instability (compare Figures 1 and 2). Chemical equlibrium between molten iron and silicate rock is not expected if the iron bodies are big enough. Stevenson (1990) argues that the formation of big iron particles is difficult. Moreover, this author argues that convective flow in the planet will disrupt big blobs and even frustrate their formation. However, the diapir model is attractive because it allows the formation of a planetary core on the short time scales suggested by the isotope data without requiring a completely molten planet (Stevenson, 2000). Diapirs can not only form by collection of distributed iron – by using, for instance, the percolation model – but also by formation of an iron layer at the bottom of a magma ocean after impact event during heavy bombardment and following a Rayleigh–Taylor instability.

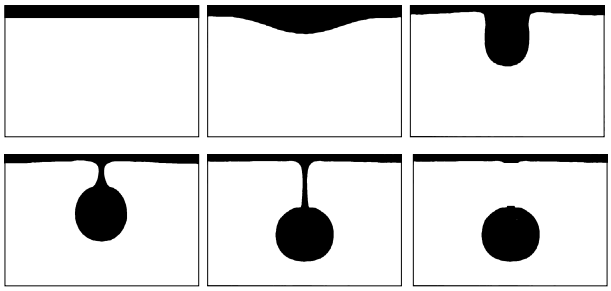

Figure 2. Sequence of different stages of formation and growth of an instability (specifically heavier material is depicted in black). In the end there is a sphere–like body which can fall towards the planet's centre.

Figure (1) illustrates how a planetary core could be formed by diapirism. After accretion the planet is a homogeneous body (1a). In the late state of accretion the speeds of impactors hitting the protoplanet's surface have increased because of the increasing mass of the protoplanet. The impact of each body heats the outer layer of the protoplanet and its outer shell starts to melt (1b). While the deep interior of the planet still has a temperature close to that of the planetary nebula, the outer shell has already a temperature higher than the melting temperature for iron or silicate and a magma ocean forms. In this magma ocean light and heavy compounds separate, where the heaviest compound (probably iron) is accumulated at the bottom of the magma ocean (1c). The overlying magma ocean starts to freeze. Since the material below the iron layer at the bottom of the frozen magma ocean is less dense than the iron there is an instable state, which will be released through a Rayleigh–Taylor instability. This instability tends to equilibrium by bringing the heavier material under the light material. On the way to the centre of the planet the falling iron collects more iron particles. After the differentiation most of the iron is concentrated in the planet's core. (1d)

The shape of a diapir depends strongly on the viscosity contrast between the two materials (Woidt, 1978). This author showed that the growing instability attains almost the shape of a perfect sphere if the penetrating material has a smaller viscosity than the surrounding material. This is actually the case for iron melt in a silicate rock environment. The spherical diapir is connected to the reservoir from which it formed by a thin chord compare Figure (2). This chord may be disrupted by convective motion in the solid but it may also help in transporting iron to the deep interior. The sinking iron diapir will heat the silicate rock by heat transfer but also as a consequence of viscous dissipation of its gravitational energy. If the viscosity of the solid rock is temperature dependent as is almost certain, the sinking iron diapir will pave the way for diapirs following it by forming a heated low viscosity channel. On the other hand the very temperature dependence of the viscosity of the rock may frustrate rapid diapir movement if the interior is cold. The interaction be the temperature dependence of viscosity and heat transfer from the diapir are, therefore, important elements of the theory of diapir core formation.

In this paper we will study how the diapir model is affected by the assumption of a temperature dependent viscosity and heat transfer from the diapir. We will solve numerically the problem of flow around a cylinder and determine the drag force on the cylinder as a function of rheology and temperature as well as the heat transfer from the cylinder to the fluid. The drag force can be equated to the body force to estimate the velocity of a sinking diapir. We study cylinders instead of spheres for simplicity. A cylinder can be treated numerically by using a 2-D code.

2. MODEL DESCRIPTION

2.1. Basic equations

We model the flow around a cylinder in a fluid with temperature dependent viscosity and solve the incompressible Navier–Stokes equations coupled with the energy and mass conservation equations. The equations are:

$$\nabla \cdot \mathbf{u} = 0 \tag{1}$$

$$\rho \frac{D\mathbf{u}}{D\,t} = -\nabla p - [\nabla \cdot \tau] + \rho g \tag{2}$$

$$\rho \frac{DT}{D\,t} = -(\nabla \cdot \mathbf{q}) - p(\nabla \cdot \mathbf{u}) - (\tau : \nabla \mathbf{u}) \tag{3}$$

where equation (1) is the continuity, (2) the momentum balance equation and (3) the energy equation. In these equations $\mathbf{u}$ denotes the velocity, p the pressure, T the temperature, g the gravity acceleration and q the heat flow. The stress tensor τ is defined as:

$$\tau_{ii} = -2\nu \frac{\partial u_i}{\partial x_i} + \frac{3}{2}\nu(\nabla \cdot \mathbf{u}), \tag{4}$$

$$\tau_{ij} = -\nu \left(\frac{\partial u_i}{\partial x_j} + \frac{\partial u_j}{\partial x_i} \right) \tag{5}$$

For the viscosity ν we assume the following weakly temperature dependent viscosity law (e.g., Turcotte & Schubert (2002)):

$$\nu(T) = \nu_0 \cdot e^{a(T-T_0)} \tag{6}$$

where ν_0 is some reference viscosity, T_0 is the maximum temperature.

2.2. Numerics

To solve the equations (1), (2), and (3) we use the finite element package FEATFLOW written by Turek

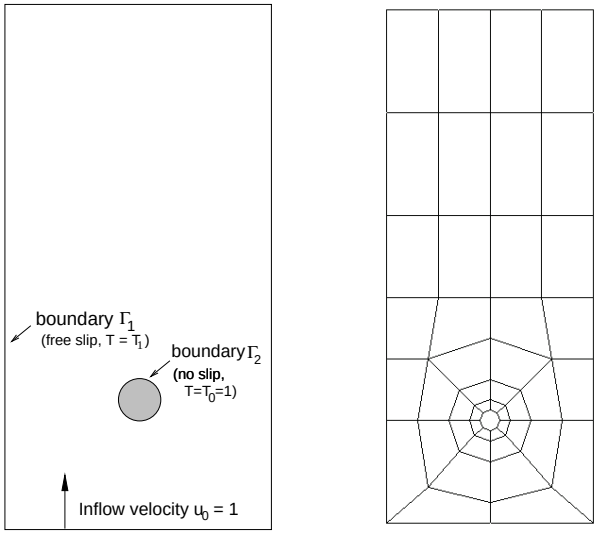

Figure 3. The setup for the model (left) and the coarse discretization (right).
Left: A single cylinder is placed in an area large enough to avoid influences from the walls. At the walls we use a free slip boundary condition; there is no friction at these boundaries. The cylinder is modeled to have a no slip boundary condition at the surface. Furthermore there is a fixed temperature at the surface of the cylinder (see section 'boundary conditions' for details).
Right: The model is discretized due to a finite element discretization with quadriliteral elements. This grid is refined during the simulation.

(1998). It is a powerful tool to solve incompressible flow problems in nonstationary flows. After discretization and refinement the equations are solved in every element due to a multigrid solver. The setup is shown in figure 3. The coarse grid is shown on the right hand side of figure 3. For the calculation and postprocessing the grid is refined up to four times; 2944 elements and 3048 knodes were calculated. Because of the immense numerical effort we use only a two dimensional model. To study the physical effects this should be sufficiant. For the future we plan to extend the model to three dimensions.

2.3. Boundary conditions

At the beginning the initial conditions $u_x = u_{x0}(x, y, t = 0)$ and $u_y = u_{y0}(x, y, t = 0)$ are given. In addition conditions at the boundaries are needed for all times. The velocity component perpendicular to the boundary is called u_n and the component tangential to the boundary u_t. We assume a 'no–slip' condition at the interface between the cylinder and the fluid and we call the outer boundary of the area Γ_1 and cylinder's surface Γ_2.

$$u_n(x,y)\Big|_{\Gamma_2} = 0, \qquad u_t(x,y)\Big|_{\Gamma_2} = 0 \tag{7}$$

At the outer boundaries of the area we use a 'free–slip' condition, there are no frictional losses along the wall:

$$u_n(x,y)\Big|_{\Gamma_1} = 0, \qquad \frac{\partial u_t(x,y)}{\partial n}\Big|_{\Gamma_1} = 0 \tag{8}$$

The inflow condition is given by both velocity components are given:

$$u_n(x, y = 0) = u_{n0}, \qquad u_t(x, y = 0) = u_{t0} \tag{9}$$

for known values for u_{n0} and u_{t0}. For the outflow condition the velocity components should not change in the direction perpendicular to the wall:

$$\frac{\partial u_n(x, y = y_{max})}{\partial n} = 0, \qquad \frac{\partial u_t(x, y = y_{max})}{\partial n} = 0 \tag{10}$$

For the temperature we use a Dirichlet' boundary condition:

$$T\Big|_{\Gamma_2} = T_0 \tag{11}$$

meaning that the temperature of the cylinder is given. The model allows to implement a time dependent function for T_0 if the temperature is to evolve in time. In this work T_0 is considered to be constant.

3. RESULTS

The flow around the cylinder shows the expected properties with respect to the streamfunction and velocity field. Figure (4a) illustrates the paths of fluid elements in a flow with low Reynolds number ($Re \leq 1$). The flow is almost symmetrical upstream and downstream, the right–hand half of figure (4a) is the mirror image of the left–hand half. The presence of the cylinder has an effect over large distances. Even many diameters away from the cylinder, the velocity is clearly different from u_0 ($u_0 = 1$) (4b). It can be shown that the highest velocity occurs at 90 degrees to the accumulation point in front of the sphere and its value is $u_{max} = 2|u_0|$

Because of viscosity there is a pressure gradient along the surface of the cylinder. A pressure gradient is

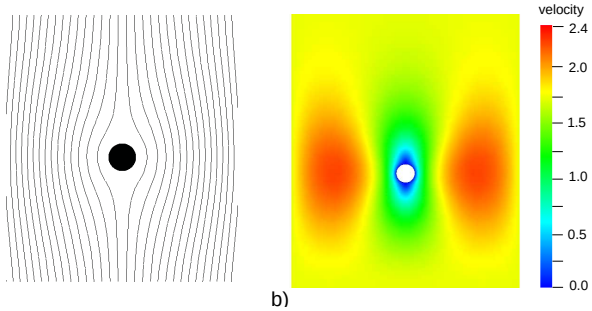

Figure 4. Flow around the cylinder; detailed view close to the cylinder. a) Streamlines for the flow around the cylinder at low Reynolds number. The lines indicate the paths of fluid elements. b) Velocity field around the cylinder. The values are nomalized to the absolute value of the inflow velocity.

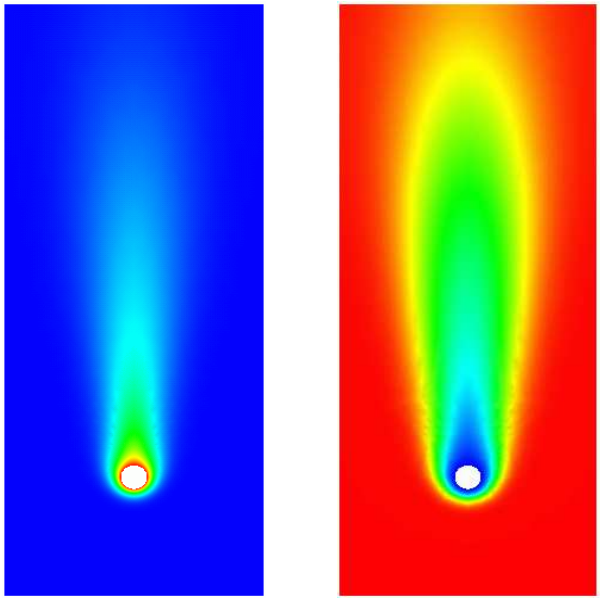

Figure 5. Temperature (left) and viscosity (right). The heat from the cylinder is transported mostly to the trailing side. As a consequence, a low-viscosity channel forms in the wake of the cylinder.

needed to move the fluid adjacent to the surface against the shear forces.

The heat of the cylinder is transported to its trailing side by the flow. A channel of higher temperature than the surrounding forms in the wake of the cylinder. Because of the temperature dependence of the viscosity a low viscosity channel forms in the wakeof the cylinder. (Fig. 5) This causes several effects: the speed of the cylinder will increase, as will the speed of possible further cylinders that may follow the first one.

Because of the temperature dependent viscosity the material close to the cylinder is less viscous compared to the material far from the cylinder, because the highest temperatures in the whole area are situated on the cylinder's surface. This causes a reduction of the shear forces and the drag force decreases. Figure 6 shows the results for the drag force for various inflow velocities. As expected the drag force is lower for a material where the viscosity decreases with rising temperature (fig. 6 solid line) than the drag force for a material having the constant viscosity of the cold material (fig. 6 dash–dotted line). Since viscous forces operate over large distances the high viscosity of the colder part of the area influences the behaviour of the material close to the cylinder. That makes clear why the drag force for the temperature dependent case is larger than the calculated drag force for a cylinder surrounded by a material with the (constant) viscosity of the maximum temperature (fig. 6 dashed line).

In figure 7 the drag forces for different viscosity contrasts are shown. A viscosity contrast of 10 is depicted in black, 100 in blue and 1000 in red. The solid

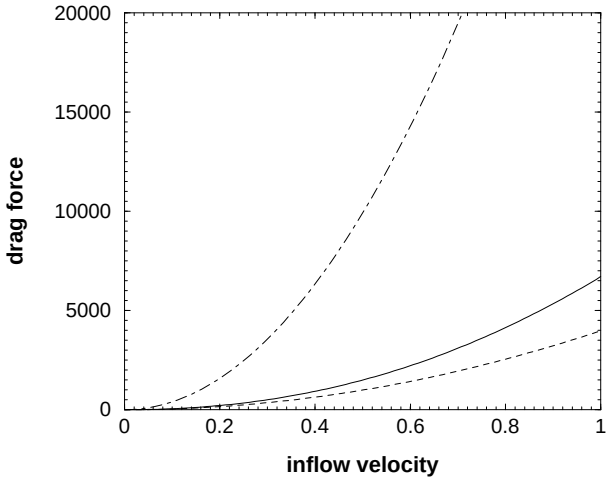

Figure 6. Drag force as a function of inflow velocity. Solid line: temperature dependent viscosity ($\nu(T_1) = 10\nu(T_0)$), dash–dottet line: $\nu = \nu(T_1)$ everywhere, dashed line: $\nu = \nu(T_0)$

lines denote the temperature dependent case and the dashed lines denote the case where the cylinder is surrounded by material with the maximum viscosity. Again the influence of viscous forces on the drag forces are higher if the viscosity contrast is larger.

4. DISCUSSION

In this paper we have shown that the drag force on a cylinder in a fluid flowing around the cylinder is substantially reduced if the viscosity is temperature dependent and if the cylinder is hotter than the ambient fluid. The factor by which the drag is reduced depends on the degree of temperature dependence of the viscosity.

These results can be applied to the problem of a cylinder and, with some reservations, to a sphere sinking in a viscous fluid. In this case, equating the drag force with the body force will allow the terminal velocity of the body under consideration to be calculated. The difference between a sphere and a cylinder is likely to be a numerical factor of order unity. Applying the results of Figure 7 to a diapir then suggests that a diapir of iron of a given size in a protoplanetary mantle will sink two to three times faster if the viscosity of the protoplanetary mantle is mildly temperature dependent with a viscosity contrast of ten. If the latter is by a factor of one hundred, the increase in sinking velocity is by a factor of four to five, and, finally, by a factor of six to seven if the viscosity contrast is by a factor of one thousand. The restricted range of values available today from the numerical calculations in terms of viscosity contrast suggests that a further increase in the temperature dependence of the viscosity will not result in much more than perhaps an order or two of magnitude increase in the sinking velocity even for very large viscosity contrasts. This result is not

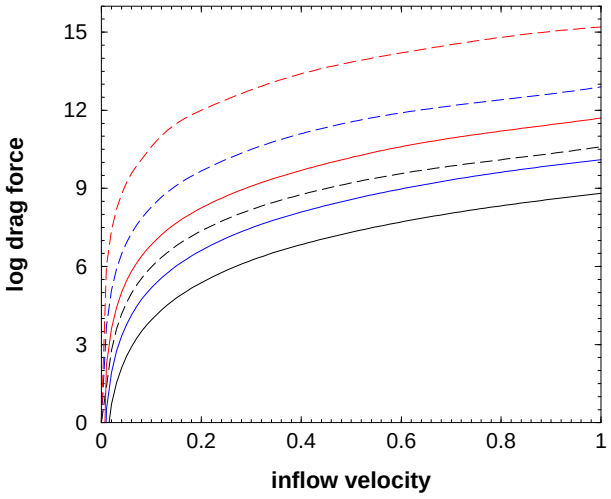

Figure 7. Drag force as a function of inflow velocity for various values of viscosity contrast between the cylinder at $T = T_0$ and the wall at $T = T_1$. The different colors are for different viscosity contrasts: 10 (black), 100 (blue) and 1000 (red). The solid lines denote the drag force for the temperature dependent viscosity, the dashed lines denote the drag force for constant viscosity $\nu = \nu(T_1)$.

unexpected since the momentum diffusion length is many times the radius of the sphere and many times larger than the thermal diffusion length. The consequence of this is that the viscosity far away from the diapir still has a substantial effect on its sinking velocity. For instance, if a 10 km radius iron diapir sinks in a 10^21 Pa s viscosity mantle by roughly 30 km than the same diapir will be expected to sink 300 km if the viscosity is strongly temperature dependent. This will allow the formation of the Earth's core in roughly 10 Ma but it is still questionable whether or not the assumed value of the viscosity is applicable and whether or not the diapirs can grow that large. After all the deep interior of the Earth or, even more likely, a small terrestrial planet may be relatively cool and more viscous assumed above. Certainly, assuming in addition a stress dependence of the rheology will help.

In the future we plan to increase the range of viscosity variations by extending the viscosity contrast due to the temperature dependence and by studying the effects of a stress dependent rheology.

Acknowledgements
We would like to thank Dominik Gödeke and Christian Becker for DeViSor, and Rainer Schmachtel for the new CC2D solver. This project is supported by the DFG.

REFERENCES

Boss, A. P., Morfill, G. E. & Tscharnuter, W. M., 1989. Models of the formation and evolution ofthe solar nebula. In S. K. Attreya, J. B. Pollack & M. S. Matthews, Eds., *Origin and Evolution of Planetary and Satellite Atmospheres*, S. 35–77. Univ. of Arizona, Tucson.

Cameron, A., 1997. The origin of the Moon and the Single Impact Hypothesis. *Icarus*, **126**, 126–137.

Cameron, A. G. W., Fegley, B., Benz, W. & Slattery, W. L., 1988. The strange density of Mercury: Theoretical considerations. In F. Vilas, C. R. Chapman & M. S. Matthews, Eds., *Mercury*, S. 692–708. Univ. of Arizona, Tucson.

Halliday, A. N. & Lee, D. C., 1999. Tungsten Isotopes and the Early Development of the Earth and Moon. *Geochim. Cosmochim. Acta*, **63**, 4157–4179.

Jacobs, J. A., 1987. *The Earth's Core*. Academic Press, New York, 2nd edition.

Konopliv, A. S., Binder, A. B., Hood, L. L., Kucinskas, A. B., Sjogren, W. L. & Williams, J. G., 1998. Improved Gravity Field of the Moon from Lunar Prospector. *Science*, **281**, 1476–1480.

Lee, D. C. & Halliday, A. N., 1997. Core Formation on Mars and Differentiated Asteroids. *Nature*, **388**, 854–857.

Ringwood, A., 1979. *Origin of the Earth and Moon*. Springer, New York.

Ringwood, A. E., 1984. The Earth's core: It's composition, formation and bearing upon the origin of the earth. *Proc. R. Soc. London*, **A395**.

Sohl, F. & Spohn, T., 1997. The interior structure of Mars: Implications from SNC meteorites. *J. Geophys. Res.*, **102**, 1613–1635.

Sohl, F., Spohn, T., Breuer, D. & Nagel, K., 2002. Implications from galileo observations on the interior structure and chemistry of the galilean satellite. *Icarus*, **157**, 104–119.

Spohn, T. & Breuer, D., 1998. Implications from Galileo observations on the interior structure and evolution of the Galilean satellites. In L. Celnikier & J. T. T. Van, Eds., *In Planetary Systems: the long vie*, S. 135–144. Editions Frontiere.

Spohn, T., Sohl, F. & Breuer, D., 1998. Mars. *Astron. Astrophys. Rev*, **8**, 181–235.

Stevenson, D. J., 1990. Fluid dynamics of core formation. In *Origin of the earth, H.E. Newsom and J.H. Jones, eds.*, S. 231–249. Oxford Univ.Press, New York.

Stevenson, D. J., 2000. Core Superheat. *AGU Fall Meeting Abstract*.

Turcotte, D. & Schubert, G., 2002. *Geodynamics*. John Wiley and Sons, London, 2nd edition.

Turek, S., 1998. *Efficient solvers for inkompressible flow problems: An algorithmic approach in view of computational aspects*. Springer.

van Bargen, N. & Waff, H. S., 1986. Permeabilities, interfacial areas and curvatures of partially molten systems: Results of numerical computations of equilibrium microstructures. *J. Geophys. Res.*, **91**, 9261–9276.

van Bargen, N. & Waff, H. S., 1988. Wetting of enstatite by basaltic melt at 1350c and 1.0 to 2.5 gpa pressure. *J. Geophys. Res.*, **93**, 1153–1158.

Vila, F., Chapman, C. R. & Matthews, M. S., 1988. *Mercury*. Arizona Univ. Press.

Wasson, J. T., 1988. The building stones of the planets. In F. Vilas, C. R. Chapman & M. S. Matthews, Eds., *Mercury*, S. 622–650. Univ. of Arizona, Tucson.

Woidt, W. D., 1978. Finite Element Calculations Applied to Salt Dome Analysis. *Tectonophysics*, **50**, 369–386.